OPEN ACCESS
Journal of Innovative Optical Health Sciences
Vol. 15, No. 5 (2022) 2250028 (13 pages)

DOI: 10.1142/S1793545822500286

World Scientific
www.worldscientific.com

A smartphone-based automated fluorescence analysis system for point-of-care testing of Hg(II)

Yafei Chen*, Ke Zhang†, Yuan Liu‡ and Chunsun Zhang§,¶,‖
MOE Key Laboratory of Laser Life Science
& Institute of Laser Life Science
College of Biophotonics South China Normal University
Guangzhou 510631, P. R. China
**cyfhiggs@163.com*
†*kerozhang@126.com*
‡*ly871120231@163.com*
§*zhangcs@scnu.edu.cn*
¶*zhangcs_scnu@126.com*

Received 17 March 2022
Accepted 11 May 2022
Published 13 September 2022

This work demonstrates a smartphone-based automated fluorescence analysis system (SAFAS) for point-of-care testing (POCT) of Hg(II). This system consists of three modules. The smartphone module is used to provide an excitation light source, and to collect and analyze fluorescent images. The dark box module is applied to integrate the desired optical elements and offers a dark environment. The cost of the integrated dark box mainly includes the upper cover, box body, lower bottom, fixture and some optical elements which is about $109. The chip module is used for fluorescence sensing, which is composed of an upper plate, bottom plate and cloth-based chip. Due to the integration of multiple smartphone functions, the SAFAS eliminates the need for additional power sources, light sources and analysis systems. The dark box and upper and bottom plates are made by 3D printer. The cloth-based chip (about $0.005 for each chip) is fabricated using the wax screen-printing technique, with no need for expensive and complex fabrication equipments. To our knowledge, the cloth-based microfluidic fluorescence detection method combined with smartphone functions is first reported. By using optimal conditions, the designed system can realize the quantitative detection of Hg(II), which has a linear range of 0.001–100 $\mu g\,mL^{-1}$ and a detection limit of 0.5 $ng\,mL^{-1}$. Additionally, the SAFAS has been successfully applied for detecting Hg(II) in actual water samples, with recoveries of 100.1%–111%, RSDs of 3.88%–9.74%, and fast detection time of about 1 min. Obviously, the proposed SAFAS has the advantages of high sensitivity, wide dynamic range, acceptable reproducibility, good stability and low cost. Therefore, it is believed that the presented SAFAS has great potential to perform the POCT of Hg(II) in different water samples.

Keywords: Smartphone; automated fluorescence detection; cloth-based chip; point-of-care testing; Hg(II).

‖Corresponding author.

1. Introduction

Point-of-care testing (POCT) is a fast and convenient detection technology that uses portable instruments to test samples at sampling points.[1] It has advantages of convenient operation, rapid detection and low cost.[2,3] Therefore, it has been applied in many areas, for instance, environmental monitoring,[4] food safety inspection[5] and clinical diagnosis.[6] Over the past decades, researchers have developed a number of POCT systems, but most of them have not yet been widely accepted by the market. One of the possible reasons for this situation is that these POCT systems are not integrated and automated enough.[7] The advance of POCT is greatly limited by large benchtop analyzers, harsh experimental conditions and professionally trained operators. However, the emergence of smartphones has changed this situation. According to the statistics, the number of smartphone users throughout the world has reached hundreds of millions.[8] The smartphone not only has the essential function of interpersonal communication, but also is endowed with more special functions such as CMOS image sensor, open-source operating system, flashlight and wireless data transmission, making it adapt to the needs of automated detection.[9] Therefore, the application of smartphone to develop POCT systems has great promise.

Nowadays, a number of detection methods for smartphone-based POCT have been explored, such as colorimetry,[10] fluorescence,[11] electrochemistry,[12] electrochemiluminescence[13] and chemiluminescence.[14] Among these methods, the fluorescence detection approach is widely used because it has high sensitivity, simple operation and strong specificity.[7] Within previously reported fluorescence POCT systems, the tested sample is usually dropped in a EP tube,[15] glass chamber[16] or cuvette.[17,18] The detection systems have some disadvantages such as complex sample pretreatment, long detection time and high detection cost, and thus they are difficult to be used in resource-poor environments. To solve the problems, fiber-based microfluidic chip technologies have attracted widespread attention because of their superiorities of convenient operation, short analysis time and low cost. Recently, the number of reports about microfluidic paper-based analytical devices (μPADs) is increasing rapidly. μPADs can be used to detect glucose and cholesterol,[19] norovirus,[20] heavy metal ions[21] and so on. However, μPADs still have some problems including narrow paper selection and poor "wet-strength".[22] Cloth is not only a widely existing material in our daily life, but also has the advantage of good mechanical property. Nowadays, it has been well considered as a supporting material to fabricate cloth-based chips (i.e., microfluidic cloth-based analytical devices (μCADs)).[23] As is well known, there are few reports about cloth-based chips used for fluorescence detection. Recently, a cloth/paper hybrid microfluidic device has been proposed for fluorescence detection of Hg(II).[24] However, this analytical device needed an expensive detection instrument and had a narrow linear range. In addition, the device had three layers of paper and one layer of cloth. The three layers of paper materials were fixed with a hollow rivet. Before the sensor was used for fluorescence detection, its top paper layer needed to be rotated, while the middle layer and the bottom layer needed to be fixed. This increased the operation complexity and the possibility of inaccurate detection.

In recent decades, the problem of public environmental pollution has aroused wide concern all over the world. Mercury is currently recognized as toxic and ubiquitous pollutants, causing serious harm to biosafety.[25,26] Mercury exists in a series of forms such as organic complexes, metal oxides and ionic state. Among them, ionic state is the most stable form, and a very small amount of Hg(II) in water can also pose a serious threat to human health.[15] As a heavy metal ion, Hg(II) has strong affinity with mercaptan group in protein. The accumulation of Hg(II) in the human body may cause damage to the digestive system, respiratory system and nervous system.[27–29] The WHO limits the amount of Hg(II) in drinking water to $6\,\mu g\,L^{-1}$.[30] Traditionally, there are many detection methods for Hg(II), such as atomic absorption/emission spectroscopy (AAS/AES),[31] high performance liquid chromatography (HPLC),[32] ion chromatography ultraviolet-visible spectroscopy[12] and inductively coupled plasma-mass spectrometry (ICP-MS).[9] Although these detection methods have high accuracy and sensitivity, they require an experienced staff, professional laboratory, expensive instrument and long detection time.[12] Therefore, it is compelling to develop a POCT system for Hg(II) detection.

In this work, a novel smartphone-based automated fluorescence analysis system (SAFAS) has been developed for point-of-care detection of Hg(II), which has a smartphone module, dark box module

and chip module. The smartphone module can provide the excitation light source, and collect and analyze fluorescent images. The dark box module provides a dark environment and integrates the required optical elements. The chip module includes a housing and a cloth-based chip. The proposed SAFAS has the following attractive features. First, the built-in LED lamp of the smartphone is used as the excitation light source, without any external light source and power supply, and thus the overall energy consumption of the system is small. Second, the fluorescence signal is collected, analyzed and stored by the smartphone, so that the integration level of the system is relatively high. Third, during the test, the operator simply drops the test solution on the chip module, without the need of any pretreatment. The integration of smartphone functions makes the operation of the system simple and quick, and can realize the "sample-to-answer" test in a short time. Finally, the dark box and the housing of cloth-based chip are fabricated by the 3D printing, which have the advantages of small size, portability, low cost and on-site use. Together with these features, the SAFAS has been successfully applied to the determination of Hg(II), with acceptable sensitivity, wide dynamic range and good stability and reproducibility. To verify the feasibility of the proposed SAFAS, real sample detection has been performed by using different water samples, proving that the system can be applied for on-site detection of water samples.

2. Materials and Methods

2.1. *Design and assembly of the SAFAS system*

The SAFAS is mainly composed of a smartphone module (Huawei TAS-AL00), dark box module and chip module. The smartphone module and the dark box module are combined by a fixture. The chip module is embedded into the dark box module by an insertion track. Figure 1(a) illustrates the main characteristics of the SAFAS and the coupling between the modules. The components of each module and the connections between these components are described as follows.

The smartphone module mainly includes a smartphone LED lamp for providing an excitation

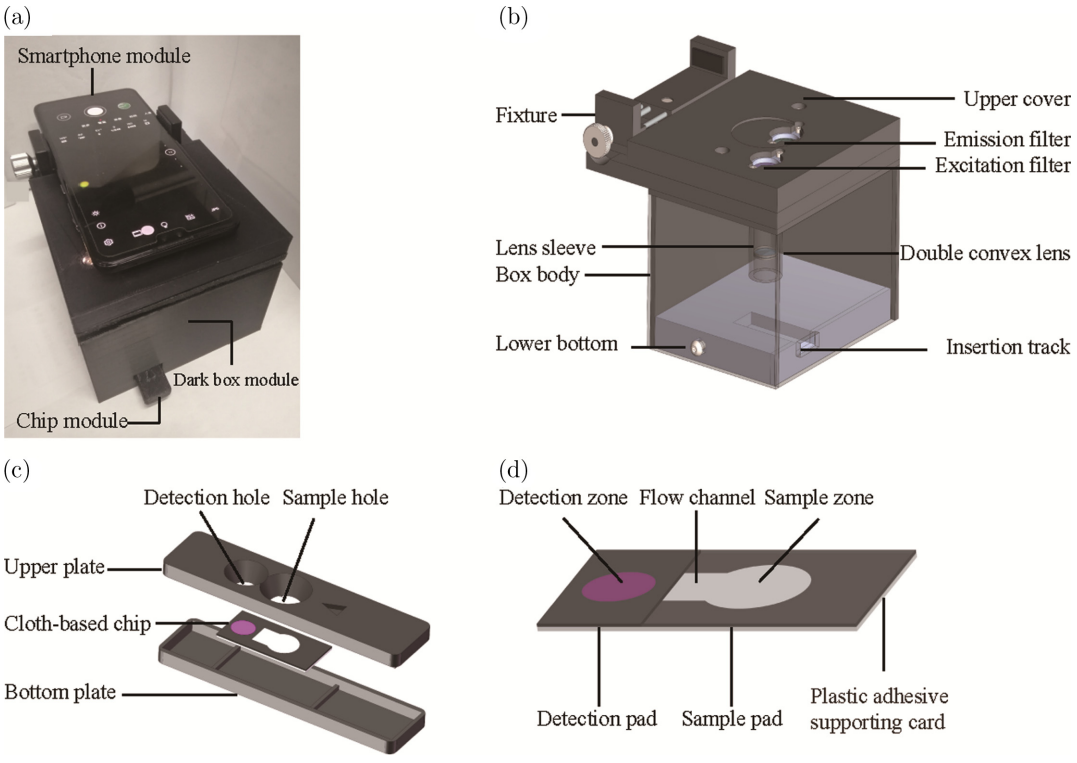

Fig. 1. Smartphone-based automated fluorescence analysis system (SAFAS). (a) Photograph of the SAFAS. The footprint of the system is 8.7 cm × 8.5 cm × 11 cm ([length] × [width] × [height]). (b) Overview of the dark box module. (c) Extended chip module assembled from the upper plate, bottom plate and the cloth-based chip. (d) Schematic of the cloth-based chip.

light source, a smartphone camera for collecting fluorescent images and an image analysis APP. The dark box module (size: 8.5 cm × 11 cm × 8.7 cm; weight: ∼380 g) was made by the 3D printer. As illustrated in Fig. 1(b), the integrated dark box module mainly comprises the upper cover, box body, lower bottom, fixture and as well some optical elements. The upper cover and lower bottom can be installed onto the box body by screws. An excitation filter, emission filter, double convex lens, lens sleeve and fixture can be assembled onto the upper cover. On the lower bottom, an insertion track is designed to provide a chip insertion port.

The box body is designed for providing a dark environment, which can prevent an external light from interfering with the internal environment to improve the signal-to-noise ratio of fluorescence detection. Additionally, it acts as a support for upper cover and lower bottom.

As shown in Fig. 1(c), the chip module (size: 6.5 cm × 5.4 cm × 0.6 cm; weight: 4.6 g), which is used for fluorescence sensing, mainly consists of cloth-based chip, upper plate and bottom plate. The upper plate and bottom plate were made by the 3D printer. The cloth-based chip is placed on the bottom plate, and then the upper plate is stuck onto the bottom plate. On the upper plate, the sample hole and detection hole are designed for adding and detecting the sample.

The layout of the cloth-based chip is shown in Fig. 1(d). The chip consists of sample pad, detection pad and plastic adhesive supporting card. The sample zone (8 mm in diameter) and the flow channel (length × width: 6 mm × 5 mm) (Fig. S1) are designed on the sample pad. The detection zone (5 mm in diameter) is devised on the detection pad. The right of the sample pad is glued to the right of the supporting card, the left of the detection pad is glued to the left of the supporting card and the right side of the detection pad partially overlaps on the sample pad. Notably, except for the smartphone, the elements of the SAFAS cost less than $109 (Table S1).

2.2. *Fabrication of the cloth-based chips*

For the chip module, one of the main components is the cloth-based chip which comprises of the detection pad and sample pad. The cloth was preprocessed to get rid of the noncellulose impurities (e.g. surface wax, pectin, etc.) and improve its hydrophilicity.[33] Briefly, the cloth was tailored into small pieces of equal size, and then they were put into a empty beaker, and be soaked in 0.1% Tween 20. Subsequently, the cloth pieces were placed in DI water to remove the remaining Tween 20, followed by being dried at room temperature. The preprocessed cloth was used for the substrate material to manufacture the cloth-based chip, unless otherwise noted.

The hydrophobic barrier patterns on the cloth-based chip were designed by Adobe Illustrator CS5 and used for the production of the screen. Figure 2 shows the detailed production steps of the cloth-based chip. First, the cloth and the wax screen were placed in turn on the automatic wax screen-printing machine, and then the machine was started. After the machine stopped, the cloth and the wax screen were placed on the heating board and then heated for about 3 s at 110°C so that the wax could fully penetrate into the cloth. Finally, they were separated from each other to get the desired cloth-based chips (Steps 1–4 in Fig. 2).

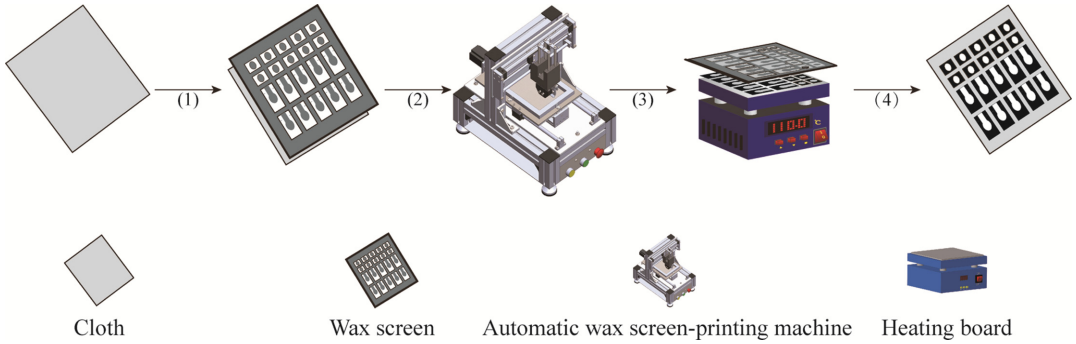

Fig. 2. Schematic illustration of the screen-printing for fabrication of cloth-based chips. (1) The cloth and the wax screen are placed in turn on the automatic wax screen-printing machine; (2) the automatic wax screen-printing machine is started; (3) the cloth and the screen are placed on the heating board; and (4) the wax screen and cloth are separated from each other.

After completion of wax screen-printing, the chip modification was performed. First, the potassium iodide (KI) solution was prepared by mixing of KI, potassium hydrogen phthalate ($C_8H_5O_4K$) and sodium thiosulfate anhydrous ($Na_2S_2O_3$) in DI water and were stirred until all the reactants dissolved in DI water completely, and then it mixed with ethylenediaminetetraacetic acid (EDTA, pH 8.0) solution in a ratio of 5:2 (v/v). Second, 28 μL of mixed solution was dropped into the sample channel and 10 μL of the Rhodamine 6G (Rh6G) solution was modified onto the detection zone. Third, the resulting cloth-based pads was placed at 37°C and vacuum-dried for 8 h. Finally, these cloth-based pads were stored in vacuum at 4°C and protected from light. As is shown in Table S2, it is necessary to note that the as-assembled cloth-based chip was very inexpensive (about $0.005 for each chip).

2.3. *Development of the image analysis APP*

The color information of the collected images are stored as R, G and B color channels, accepting the value range between 0 and 255. To convert a smartphone into a data processing system, the APP based on the Android Studio development platform was developed. The opensource library was used to develop the APP based on the standard curve algorithm. Briefly, the APP fixes the size of the fluorescent image that is cropped each time to 70 × 70 px, and the fluorescent image is stored as Bitmap format. Fixing the size of the picture is beneficial to eliminate the error caused by the size problem. Since the bitmaps contain rich image information and almost do not need for compression, the images in this format are usually more accurate in color data than the images in JPG format. Subsequently, the APP uses a double-layer "for" loop statement to scan the pixels of the fluorescent image from the origin of the bitmap, combines it with the Get Pixel method in the Bitmap to extract the Red value of each pixel of the fluorescent image and creates a counter to record the accumulation of the Red value of each pixel value. The average Red value is calculated according to the value accumulated by the Red value of each pixel of the fluorescent image recorded in the counter and the average value formula. The average Red value is displayed on the APP interface. The average Red value of the image is subtracted from the average Red value of the image at 0 g L^{-1} Hg(II) to obtain the Δ Red value. Then, the obtained Δ Red values are imported into Origin8.5 (MicroCal Software Inc., MA, USA) to make the related plots for further analysis. A calibration equation has been obtained by recording the fluorescence emission from standard sample solutions. After that, Hg(II) concentration of unknown samples can be estimated through the Δ Red channel intensity in the calibration equation. The home page, detection and data recording interfaces of the APP are shown in Fig. S2. A user needs to press the 'Photo' tab in the home page of the APP to select the measured photo. After selecting this photo, a new panel will pop-up and the user can select the zone to be detected. Finally, the user only needs to click "Yes" and the concentration of Hg(II) is displayed on the data recording interface.

2.4. *Analytical procedure*

After the construction of the SAFAS, the system could be carried out to detect Hg(II) concentration. The detailed operation procedures are as follows. The tested sample solution was dropped into the sample hole. After that, due to the action of capillary force, the sample solution quickly flowed laterally through the sample channel and then into the detection zone to trigger the fluorescence reaction. After a length of reaction time, the chip module was well embedded into the box module. Next, the fluorescence signals could be captured by the smartphone camera, and the APP could automatically analyze the captured image to determine the concentration of Hg(II). The image capture settings of the camera were set as follows: f/400 aperture, ISO ~6400, 1x focal length of the camera lens and WB ~4000.

3. Results and Discussion

3.1. *Detection principle of the SAFAS*

For the presented analysis, a previously reported chemical protocol[18] was applied for detecting the concentration of Hg(II). The tested sample solution containing Hg(II) was dropped into the sample zone. During lateral flow, Hg(II) reacted with excess KI on the sample pad and generated KCl and tetraiodomercurate (II) (HgI_4^{2-}) ions. The solution containing HgI_4^{2-} further flowed into the detection zone and reacted with Rh6G to generate a complex ternary compound. This substance did not emit

fluorescence, and the fluorescence property of Rh6G was gradually quenched as the concentration of Hg(II) increased.

As shown in Fig. S3, the fluorescence of Rh6G was excited by the smartphone LED. The excitation light was filtered by a 500–540 nm band-pass filter and then converged through a double convex lens to form a small green bean spot to stimulate the fluorescent substance in the detection area of the cloth-based chip. By optimally selecting the double convex lens (i.e., focal length of 25 mm and lens diameter of 12.5 mm), the distances between the lens and the light source and as well between the lens and the detection zone were about 25 mm and 30 mm, respectively. As a result, the diameter of bean spot was set as about 5 mm, which could well excite the whole detection zone. The light emitted from the detection area passed through a 545 nm emission filter and was collected by the smartphone camera to form a yellow-green fluorescent image. In the proposed SAFAS, the intensity of fluorescence emission from the Rh6G could be well correlated with the concentration of Hg(II).

3.2. *Optimization of the cloth-based chip*

For the chips, the tested sample solution can flow into the detection zone by capillary force, without the need for additional pumping equipment. Therefore, the size of the suitable flow channel should be devised to acquire the desired fluorescence determination. Figure 3(a) shows the effect of channel width on the flow time. The flow time was defined as the time when the detection zone was filled with the sample solution. Obviously, the width of the flow channel greatly affected the flow time required for the dye liquid to flow throughout the detection zone. Based on the shortest flow time and the resulting reduction of detection time, the width of the flow channel was selected to be 5 mm.

Additionally, the length of the flow channel was also very much linked with the fluorescence intensity. Figure 3(b) shows the dependence of the fluorescent signal on the flow channel length in the range of 1–26 mm. As seen from Fig. 3(b), a maximum Δ Red channel intensity was obtained at 6 mm, as such the length of 6 mm as the best length for this work. In short, the flow channel with 5 mm width and 6 mm length was chosen for all late experiments.

3.3. *Optimization of the test parameters*

Further, the concentration of KI ([KI]), concentration of EDTA ([EDTA]), concentration of Rh6G ([Rh6G]) and the time from sampling to detection ($t_{s\text{-}d}$) should be optimized. As is well known, the [KI] has an important influence on the presented fluorescent detection. In our case, its values were examined in the range of 2–40 g L^{-1}. As shown in Fig. 4(a), the Δ Red channel intensity was increased as the [KI] was enhanced. However, at higher

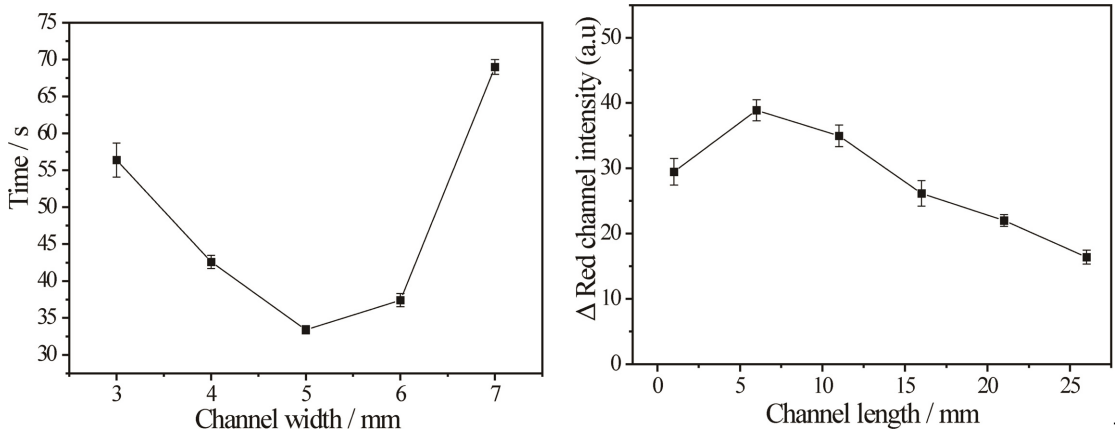

Fig. 3. Effect of channel width on the flow time (a) and effect of channel length on the Δ Red channel intensity (b). In panel (a), carmine volum-40 μL, channel length-11 mm, channel width-3–7 mm. In panel (b), [Hg(II)]-50 μg mL^{-1}, sample volum-40 μL, channel width-5 mm, channel length-1–26 mm, [KI]-10 g L^{-1}, [EDTA]-15 g L^{-1}, [Rh6G]-0.2 g L^{-1} and $t_{s\text{-}d}$ − 2 min.

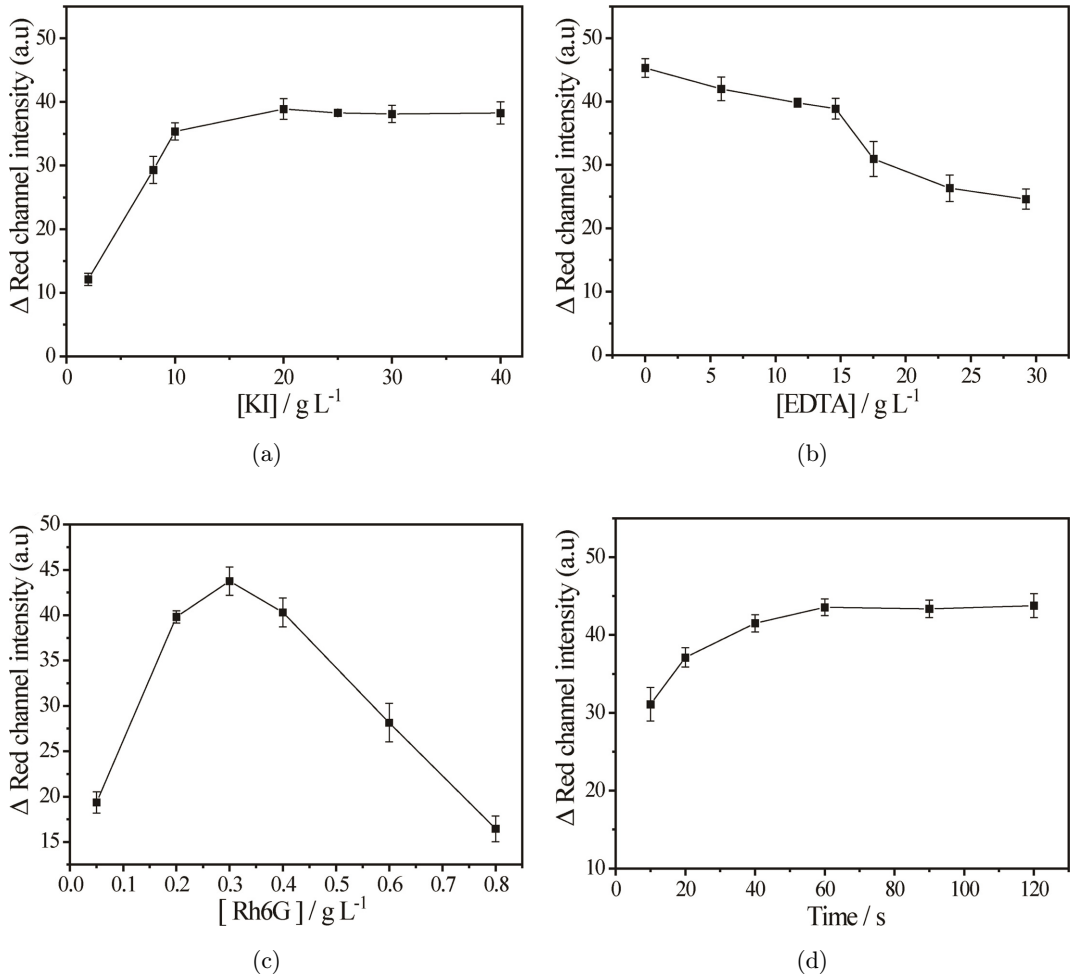

Fig. 4. Effects of concentration of KI ([KI]), (a) concentration of EDTA ([EDTA]), (b) concentration of Rh6G ([Rh6G]), (c) and $t_{s\text{-}d}$ (d) on the Δ Red channel intensity. In panel (a), [Hg(II)]-50 μg mL^{-1}, sample volume-40 μL, channel width-5 mm, channel length-6 mm, [KI]-2–40 g L^{-1}, [EDTA]-15 g L^{-1}, [Rh6G]-0.2 g L^{-1} and $t_{s\text{-}d}$-2 min. In panel (b), [Hg(II)]-50 μg mL^{-1}, sample volume-40 μL, channel width-5 mm, channel length-6 mm, [KI]-10 g L^{-1}, [EDTA]-0-30 g L^{-1}, [Rh6G]-0.2 g L^{-1} and $t_{s\text{-}d}$-2 min. In panel (c), [Hg(II)]-50 μg mL^{-1}, sample volume-40 μL, channel width-5 mm, channel length-6 mm, [KI]-10 g L^{-1}, [EDTA]-12 g L^{-1}, [Rh6G]-0.05-0.8 g L^{-1} and $t_{s\text{-}d}$-2 min. In panel (d), [Hg(II)]-50 μg mL^{-1}, sample volume-40 μL, channel width-5 mm, channel length-6 mm, [KI]-10 g L^{-1}, [EDTA]-12 g L^{-1}, [Rh6G]-0.3 g L^{-1} and $t_{s\text{-}d}$ – 10–120 s. The error bars represent the standard deviations of five independent measurements.

concentrations greater than 10 g L^{-1}, the Δ Red channel intensity appeared to have reached a plateau. The possible reason for this phenomenon is that at low concentrations of I^-, I^- combines with Hg(II) to form HgI_3^- which is very weak in nature, and the more stable species is HgI_4^{2-} formed at high concentrations of I^-.[34] Therefore, 10 g L^{-1} KI was selected as the optimized concentration.

The effect of [EDTA] on the Δ Red channel intensity was evaluated by adding EDTA to the KI solution. Figure 4(b) shows that in the presence of 5, 12 or 15 g L^{-1} EDTA, the Δ Red channel intensity did not decrease significantly. However, the fluorescence signal was observed to decrease obviously when the [EDTA] values were great than or equal to 18 g L^{-1}. Therefore, in samples with different interference levels, 5–15 g L^{-1} EDTA may be selected to mask metal ions.

For the SAFAS, Rh6G served as a fluorescent reagent, and thus the Δ Red channel intensity is greatly related to the [Rh6G]. As shown in Fig. 4(c), the Δ Red channel intensity gradually enhanced in the range of 0.05–0.3 g L^{-1}. However, when the [Rh6G] value ranged from 0.3 to 0.8 g L^{-1}, the fluorescence signal gradually decreased, possibly because the quenching occurred due to the collision mechanism between the excited state molecules and ground state molecules.[35]

For the cloth-based fluorescence detection, the time when the sample solution flowed through the hydrophilic zone until the fluorescence signal was measured might be an important parameter affecting the Δ Red channel intensity. For evaluating this time, the values of $t_{s\text{-}d}$ were optimized in the range of 10–120 s. It can be seen from Fig. 4(d) that the Δ Red channel intensity was enhanced step by step when the $t_{s\text{-}d}$ varied from 10 to 60 s, and then reached a plateau at time lengths longer than 60 s. This phenomenon might be explained by the fact that the sample solution could be well filled with the detection zone and the fluorescence reaction performed enough. Therefore, the optimal $t_{s\text{-}d}$ value was chosen to be 60 s.

3.4. *Analytical sensitivity, reproducibility and selectivity*

The analytical performance of the SAFAS for Hg(II) was investigated under optimized conditions. Figure 5 shows the relationship between the Δ Red channel intensity and Hg(II) concentration. Obviously, the Δ Red channel intensity increased with Hg(II) concentration in the range of 0.001–100 μg mL^{-1}, implying that the SAFAS could perform quantitative Hg(II) measurement (Fig. 5(a)). The corresponding typical fluorescent images are shown in Fig. S4. It was observed that the fluorescence signal varied linearly with the logarithms of the Hg(II) concentration ranging from 0.001 to 100 μg mL^{-1} with a squared correlation coefficient ($R^2 = 0.9901$, $n = 5$) (Fig. 5(b)). The limit of detection of (LOD) was estimated to be 0.5 ng mL^{-1}. Here, the LOD was defined as the lowest Hg(II) concentration that generated a signal three standard deviations higher than the background signal. Thus, the detection sensitivity allowed the measurement of allowable concentration of Hg(II) in drinking water (2 ng mL^{-1} and 6 ng mL^{-1} fixed by U.S. Environmental Protection Agency and the World Health Organization, respectively[27]). Reproducibility of the SAFAS's fluorescence response was assessed as the relative standard deviation (RSD) of five independent measurements of 0.001, 0.005 and 0.01 μg mL^{-1} Hg(II). The corresponding RSD values were determined to be 12.07%, 7.02% and 4.31%. These results showed that the SAFAS could be used for the accurate and sensitive determination of Hg(II) in environmental water samples in the future.

It is fundamental to have good anti-interference capability for a reliable and applicable detection system. In the present case, the anti-interference capability of the SAFAS has been evaluated by testing several common potential interfering ions (Na^+, K^+, Zn^{2+}, Cu^{2+}, Fe^{2+}, Mg^{2+}, Ca^{2+}, Fe^{3+}, Cr^{3+}). The Δ Red channel intensity of the Hg(II) solution containing a certain foreign species was compared with that without any foreign species. The foreign metal ions were regarded as noninterference when the influence of the foreign metal ions

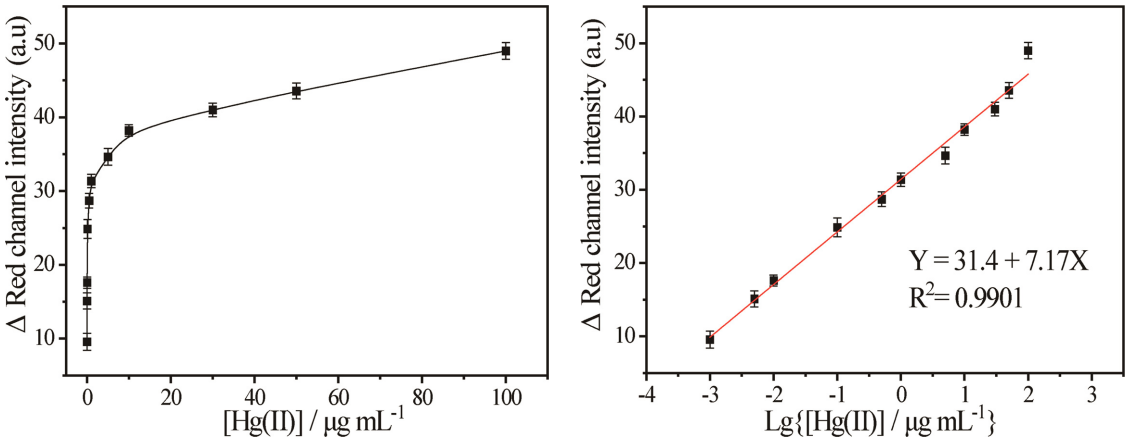

(a) (b)

Fig. 5. (a) Calibration curve for determination of [Hg(II)] using the SAFAS ([Hg(II)]-0, 0.001, 0.005, 0.01, 0.1, 0.5, 1, 5, 10, 30, 50 and 100 μg mL^{-1}). (b) Linear relationship between Δ Red channel intensity and logarithms of [Hg(II)]. Experimental conditions: Sample volume-40 μL, channel width-5 mm, channel length-6 mm, [KI]-10 g L^{-1}, [EDTA]-12 g L^{-1}, [Rh6G]-0.3 g L^{-1} and $t_{s\text{-}d}$-60 s. The error bars represent the standard deviations of five independent measurements.

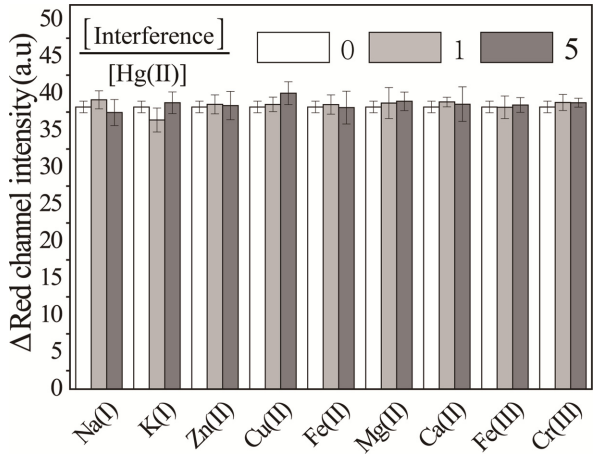

Fig. 6. Evaluation of selectivity of the SAFAS. Experimental conditions: Sample volume-40 μL, [Hg(II)]-10 μg mL^{-1}, channel width-5 mm, channel length-6 mm, [KI]-10 g L^{-1}, [EDTA]-12 g L^{-1}, [Rh6G]-0.3 g L^{-1} and $t_{s\text{-}d}$-60 s. The error bars represent the standard deviations of five independent measurements.

on Red value was less than 3 s (s represented the standard deviation of the assay of Hg(II) solution in the absence of interfering ion). Figure 6 shows the detection of 10 μg mL^{-1} Hg(II) in the EDTA (12 g L^{-1})-modified cloth-based chip. Obviously, it was considered noninterference when the concentration ratio of foreign ions and Hg(II) was 1:1. And, even when the concentration ratio of foreign ions and Hg(II) was 5:1, it did not interfere with the corresponding analysis of the system. Therefore, the proposed SAFAS can provide highly selective determination of Hg(II) in water samples with different pollution levels.

3.5. *Determination of Hg(II) in real water sample*

To prove the feasibility of the SAFAS, the SAFAS was assessed for detecting Hg(II) in actual samples including tap water, polluted water and sea water samples. Two Hg(II) concentrations of 0.1 μg mL^{-1} and 10 μg mL^{-1} were spiked to the actual samples, and tested using the SAFAS and ICP-MS in parallel. According to Table 1, Hg(II) in three different water samples could be detected. The recovery experiments by the SAFAS demonstrated the receivable data of the different water samples, with recoveries of 106–111% for 0.1 μg mL^{-1} Hg(II) (6.56–9.74% RSD), and of 100.1–103.9% for 10 μg mL^{-1} Hg(II) (5.77–9.74% RSD). Water samples were also subjected to ICP-MS detection of Hg^{2+} as a reference, and it revealed that the SAFAS results had a good agreement with that of the ICP-MS. Therefore, the developed SAFAS had an acceptable feasibility for detection of Hg(II) concentration, with advantages of small size, portability, low cost and on-site use.

3.6. *On-site detection of Hg(II)*

To prove the POCT of Hg(II) by the SAFAS, the SAFAS was assessed for detecting Hg(II) at three different areas including the South China Normal University, Pearl River and Jiang Men Zhong Huan Detection Technology Co., Ltd. Figure S5 shows on-site locations for monitoring the contamination of Hg(II) by the SAFAS. Water samples collected at those three locations were also subjected to the atomic fluorescence spectrometer (AFS) for detection of Hg(II) as a reference. As shown in Table 2, no Hg(II) was detected in tap water from South China Normal University and water in the Pearl River, which verified that these two water samples were not polluted. However, the concentration of Hg(II) in the sample of Jiang Men Zhong Huan Detection Technology Co., Ltd. was in the range of 0.0132 $\pm$ 0.0025 μg mL^{-1}. Importantly, the results

Table 1. Determination of Hg(II) in three water samples.

	Hg(II) added (μg mL^{-1})	Hg(II) found (μg mL^{-1})	Recovery (%)	RSD (%, $n = 5$)	ICP-MS results (μg mL^{-1})
Tap water	0.1	0.11	111	7.83	0.102
	10	10.01	100.1	5.77	10.093
Sea water	0.1	0.106	106	6.56	0.101
	10	10.39	103.9	3.88	10.009
Polluted water	0.1	0.11	110	9.74	0.114
	10	10.34	103.4	7.54	10.121

Note: The assay conditions were as follows: Sample volume-40 μL, channel width-5 mm, channel length-6 mm, [KI]-10 g L^{-1}, [EDTA]-12 g L^{-1}, [Rh6G]-0.3 g L^{-1} and $t_{s\text{-}d}$-60 s. The RSD was from five independent measurements.

Table 2. Determination of Hg(II) in water samples in three different areas.

Area	Metal ion	Detected by the SAFAS (μg mL^{-1})	RSD (%, $n = 5$)	Detected by the AFS (μg mL^{-1})
South China Normal University	Hg(II)	ND		ND
Pearl River	Hg(II)	ND		ND
Jiang Men Zhong Huan Detection Technology Co., Ltd	Hg(II)	0.0132 ± 0.0025	19.27	0.014

Note: The assay conditions were as follows: Sample volume-40 μL, channel width-5 mm, channel length-6 mm, [KI]-10 g L^{-1}, [EDTA]-12 g L^{-1}, [Rh6G]-0.3 g L^{-1}, and $t_{s\text{-}d}$-60 s. The relative standard deviation (RSD) was from five independent measurements.

obtained by the SAFAS had a good agreement with that of the AFS. Therefore, the proposed SAFAS had the potential for on-site detection of Hg(II) in water samples.

3.7. *Differences in performance between highly trained users and fully untrained users*

To prove the SAFAS was user friendly and did not need complex sample preparation, three fully untrained users (people who lack scientific training, but can read an instruction manual on how to operate the device) were invited to perform the SAFAS for detection of Hg(II). Each volunteer was given an instruction manual which is shown in the Supporting Information. As shown in Table 3, the results detected by the author and volunteers were highly consistent. In addition, there was no obvious difference in total detection time. Therefore, the developed SAFAS was user friendly, with no need of experienced operation staff.

3.8. *Storage stability of the chip module*

The storage stability of the chip module is an important factor affecting its application and development. To assess this, the cloth-based chips were vacuum-packed in a foil bag and stored at 4°C. In this study, the chips were tested every week for about three months. Figure 7 shows that the signal intensities could retain 95.13%, 91.77% and 82.67% of their initial signal after three, six and twelve weeks, respectively. These data indicated that the chip module had an acceptable storage stability.

Table 3. Differences in performance between highly trained users and fully untrained users.

Operator	Result (μg mL^{-1})	RSD (%)	Average testing time (s)	RSD (%)
Author	0.108	13.76	74.8	1.11
Volunteer 1	0.112	15.67	75.6	1.50
Volunteer 2	0.114	14.85	76.4	1.49
Volunteer 3	0.117	15.38	75.4	1.51

Note: The assay conditions were as follows: [Hg(II)]-0.1 μg mL^{-1}, sample volume-40 μL, channel width-5 mm, channel length-6 mm, [KI]-10 g L^{-1}, [EDTA]-12 g L^{-1}, [Rh6G]-0.3 g L^{-1}, and $t_{s\text{-}d}$-60 s. The relative standard deviation (RSD) was from five independent measurements.

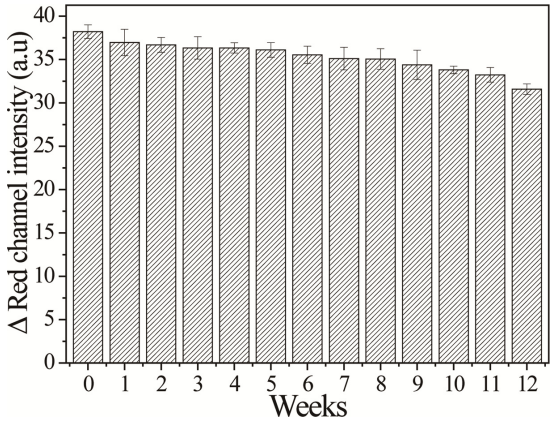

Fig. 7. Storage stability of the chip module. Experimental conditions: Sample volume-40 μL, [Hg(II)]-10 μg mL^{-1}, channel width-5 mm, channel length-6 mm, [KI]-10 g L^{-1}, [EDTA]-12 g L^{-1}, [Rh6G]-0.3 g L^{-1} and $t_{s\text{-}d}$-60 s. The error bars represent the standard deviations of five independent measurements.

3.9. *Comparison of the proposed method and other smartphone-based methods for detection of Hg(II)*

In recent years, different smartphone-based detection methods have been designed for Hg(II) detection (Table S3). For instance, Chen's group developed a paper-based analytical devices using gold nanoparticles as a colorimetric sensing strategy, where the determination of Hg(II) with a detection limit of 10 ng mL^{-1} was obtained in 40 min.[36]

Nguyen and coworkers presented the smartphone-based nano colorimetry for detection of Hg(II), where the glass-PDMS microfluidic device was constructed and the detection limit of $1.4\,ng\,mL^{-1}$ was obtained in 10 min.[25] Different from the smartphone-based colorimetric systems, a smartphone-based electrochemical POCT system has been proposed by Xu *et al.* for detection of Hg(II), which has a detection limit of $7.0\,ng\,mL^{-1}$ and detection time of 12 min.[12] This system consisted of a handheld electrochemical analyzer, a smartphone installed with an APP DHMI and a customized screen-printed carbon electrode. Recently, the smartphone-based fluorescent POCT systems also attract much attention. Hatiboruah's group developed a fluorescent sensing system for determination of Hg(II),[18] where the detection limit of $32\,ng\,mL^{-1}$ and detection time of 15 min were achieved. A smartphone-based optical fiber fluorescence sensor has been proposed by Liu and coworkers, and it has a detection limit of $0.2\,ng\,mL^{-1}$ and needs 3 min for Hg(II) detection.[15] The cost of a single test is about \$2.29, which is much higher than the SAFAS's cost per test. Although this fluorescence sensor has a slightly lower detection limit than the SAFAS, the modification processes of the fiber probes are complex. First, the fabricated combination tapered fiber probes were immersed into the piranha solution for 30 min, then they needed to be washed and air-dried. Second, they were salinized into the triethoxysilane/isopropyl alcohol for 2 h and dried in the oven at 80°C for 2 h. Third, the fiber probes were immersed into the specific mixture for 4 h, and kept in dark. Finally, they needed to be immersed into bovine serum albumin (BSA) solution for 1 h. These operations undoubtedly increase the labor and time cost. Shan and coworkers described a smartphone-based method for Hg(II) detection,[16] which had a detection limit of $0.2\,ng\,mL^{-1}$ and needed at least 30 min. For this method, the test solution was mixed with two different reagents and incubated at room temperature for 20 min. Next, the incubated products needed to be cleaned three times with a magnetic separation device. Finally, the precipitate was suspended with a buffer and applied to the glass sample chamber for collection of fluorescence signals. Obviously, the detection processes of this method are relatively complex. In short, the above-mentioned smartphone-based detection methods have been desirably used for Hg(II) determination. However, they still have several disadvantages including: (1) All of them require relatively complex preprocesses, which increases the difficulty in sample and data processing and the detection time; (2) most of them have a high detection limit, which is not sensitive to Hg(II) detection; (3) the sensor interfaces for these systems are usually high in cost or complex in preparation. On the contrary, the proposed SAFAS for point-of-care testing of Hg(II) can effectively overcome these shortcomings. It only requires a simple operation, and can perform the sample-to-answer detection in 1 min. Additionally, it just needs the ultra-cheap and easy-to-prepare cloth-based chip (about \$0.005 for each chip), and as well inexpensive components (less than \$109 except the smartphone). As described above, the SAFAS can offer a lower detection limit and high specificity. Therefore, the SAFAS has the great potential for accurate, rapid and sensitive on-site Hg(II) monitoring in resources-limited environments.

4. Conclusions

In summary, the presented work has realized the integration of fluorescence detection, cloth-based microfluidics and smartphone-based light excitation and collection to build a SAFAS for point-of-care detection of Hg(II). A custom designed APP has been developed, which can analyze fluorescent images and convert them into corresponding Hg(II) concentrations. By using this SAFAS, the concentrations of Hg(II) in water can be detected on site in real time. The detection limit of Hg(II) is low to be $0.5\,ng\,mL^{-1}$, and the testing process can be completed in about 1 min. Importantly, the detection results on the SAFAS are consistent with those by using the traditional instrument. Looking to the future, the SAFAS should have the potential to provide POCT for Hg(II) in different water samples. In addition, we believe the SAFAS is an enabling system, which can find broad applications in point-of-care medical diagnostics, environmental testing and food safety inspection.

Conflict of Interest

The authors declare that there are no conflict of interest related to this paper.

Acknowledgments

This research is supported by the Guangdong Basic and Applied Basic Research Foundation

(2019A1515011284) and Guangzhou Basic and Applied Basic Research Foundation (202002030265).

References

1. B. X. Lin, Y. Yu, Y. J. Cao, M. L. Guo, D. B. Zhu, J. X. Dai, M. S. Zheng, "Point-of-care testing for streptomycin based on aptamer recognizing and digital image colorimetry by smartphone," *Biosens. Bioelectron.* **100**, 482–489 (2018).
2. F. Katzmeier, L. Aufinger, A. Dupin, J. Quintero, M. Lenz, L. Bauer, S. Klumpe, D. Sherpa, B. Dürr, M. Honemann, I. Styazhkin, F. C. Simmel, M. Heymann, "A low-cost fluorescence reader for *in vitro* transcription and nucleic acid detection with Cas13a," *Plos One* **14**, e0220091 (2019).
3. T. Liu, W. Q. Wang, H. Ding, D. R. Yi, "Smartphone-based hand-held optical fiber fluorescence sensor for on-site pH detection," *IEEE Sens. J.* **19**, 9441–9446 (2019).
4. J. N. Wang, Z. L. Xia, Y. Su, M. C. Lu, Y. Wan, Y. He, "Handheld, one-step, and rapid electrochemical biosensor platform with smartphone interface," *Appl. Mech. Mater.* **868**, 340–344 (2017).
5. K. Y. Wang, Z. H. Wang, H. Zeng, X. L. Luo, T. Yang, "Advances in portable visual detection of pathogenic bacteria," *ACS Appl. Bio Mater.* **3**, 7291–7305 (2020).
6. S. Ghosh, K. Aggarwal, T. U. Vinitha, T. Nguyen, J. Y. Han, C. H. Ahn, "A new microchannel capillary flow assay (MCFA) platform with lyophilized chemiluminescence reagents for a smartphone-based POCT detecting malaria," *Microsyst. Nanoeng.* **6**, 2–18 (2020).
7. J. J. Liu, Z. X. Geng, Z. Y. Fan, J. Liu, H. D. Chen, "Point-of-care testing based on smartphone: The current state-of-the-art (2017–2018)," *Biosens. Bioelectron.* **132**, 17–37 (2019).
8. Y. Fan, J. T. Liu, Y. Wang, J. P. Luo, H. R. Xu, S. W. Xu, X. X. Cai, "A wireless point-of-care testing system for the detection of neuron-specific enolase with microfluidic paper-based analytical devices," *Biosens. Bioelectron.* **95**, 60–66 (2017).
9. M. Xiao, Z. G. Liu, N. X. Xu, L. L. Jiang, M. S. Yang, C. Q. Yi, "A smartphone-based sensing system for on-site quantitation of multiple heavy metal ions using fluorescent carbon nanodots based microarrays," *ACS Sens.* **5**, 870–878 (2020).
10. S. Sajed, F. Arefi, M. Kolahdouz, M. A. Sadeghi, "Improving sensitivity of mercury detection using learning based smartphone," *Sens. Actuat. B* **298**, 126942 (2019).
11. Y. Gong, Y. M. Zheng, B. R. Jin, M. L. You, J. Y. Wang, X. J. Li, M. Li, F. Xu, F. Li, "A portable and universal upconversion nanoparticle-based lateral flow assay platform for point-of-care testing," *Talanta* **201**, 126–133 (2019).
12. Z. Z. Xu, Z. J. Liu, M. Xiao, L. L. Jiang, C. Q. Yi, "A smartphone-based quantitative point-of-care testing (POCT) system for simultaneous detection of multiple heavy metal ions," *Chem. Eng. J.* **394**, 124966–124975 (2020).
13. S. Li, J. L. Liu, Z. Chen, Y. L. Lu, S. S. Low, L. H. Zhu, C. Cheng, Y. He, Q. M. Chen, B. Su, Q. J. Liu, "Electrogenerated chemiluminescence on smartphone with graphene quantum dots nanocomposites for Escherichia Coli detection," *Sens. Actuators B* **297**, 126811 (2019).
14. T. H. Fereja, S. A. Kitte, W. Y. Gao, F. Yuan, D. Snizhko, L. M. Qi, A. Nsabimana, Z. Y. Liu, G. B. Xu, "Artesunate-luminol chemiluminescence system for the detection of hemin," *Talanta* **204**, 379–385 (2019).
15. T. Liu, W. Q. Wang, D. Jian, J. H. Li, H. Ding, D. R. Yi, F. Liu, S. Y. Wang, "Quantitative remote and on-site Hg^{2+} detection using the handheld smartphone based optical fiber fluorescence sensor (SOFFS)," *Sens. Actuators B* **301**, 127168 (2019).
16. Y. K. Shan, B. Wang, H. C. Huang, D. Jian, X. P. Wu, L. A. Xue, S. Y. Wang, F. Liu, "On-site quantitative Hg^{2+} measurements based on selective and sensitive fluorescence biosensor and miniaturized smartphone fluorescence microscope," *Biosens. Bioelectron.* **132**, 238–247 (2019).
17. L. Wang, B. Q. Li, F. Xu, X. Y. Shi, D. M. Feng, D. Q. Wei, Y. Li, Y. J. Feng, Y. M. Wang, D. C. Jia, Y. Zhou, "High-yield synthesis of strong photoluminescent N-doped carbon nanodots derived from hydrosoluble chitosan for mercury ion sensing via smartphone APP," *Biosens. Bioelectron.* **79**, 1–8 (2016).
18. D. Hatiboruah, T. Das, N. Chamuah, D. Rabha, B. Talukdar, U. Bora, K. U. Ahamad, P. Nath, "Estimation of trace-mercury concentration in water using a smartphone," *Measurement* **154**, 107507 (2020).
19. L. Guo, S. A. Chen, Y. L. Yu, J. H. Wang, "A smartphone optical device for point-of-care testing of glucose and cholesterol using Ag NPS/ Uio-66-NH2-based ratiometric fluorescent probe," *Anal. Chem.* **93**, 16240–16247 (2021).
20. S. Chung, L. E. Breshears, A. Gonzales, C. M. Jennings, C. M. Morrison, W. Q. Betancourt, K. A. Reynolds, J. Y. Yoon, "Norovirus detection in water samples at the level of single virus copies per microliter using a smartphone-based fluorescence microscope," *Nat. Protoc.* **16**, 1452–1475 (2021).
21. Q. P. Shang, P. Zhang, H. J. Li, R. Liu, C. S. Zhang, "A flow chemiluminescence paper-based microfluidic

device for detection of chromium (III) in water," *J. Innov. Opt. Heal. Sci.* **12**, 1950016 (2019).
22. J. Li, J. Jiang, Y. Su, Y. Liang, C. S. Zhang, "A novel cloth-based supersandwich electrochemical aptasensor for direct, sensitive detection of pathogens," *Anal. Chim. Acta* **1188**, 339176 (2021).
23. C. S. Zhang, Y. Su, Y. Liang, W. Lai, "Microfluidic cloth-based analytical devices: Emerging technologies and application," *Biosens. Bioelectron.* **168**, 112391 (2020).
24. L. Y. Wang, B. W. Li, J. N. Wang, J. Q. J. H. Li, J. P. Ma, L. X. Chen, "A rotary multi-positioned cloth/paper hybrid microfluidic device for simultaneous fluorescence sensing of mercury and lead ions by using ion imprinted technologies," *J. Hazard. Mater.* **428**, 128165 (2022).
25. H. Nguyen, I. Misbah, W. C. Shih, "Smartphone nano-colorimetry for on-demand multiplex lead and mercury detection and quantitation in drinking water," *IEEE Sens. J.* **20**, 6685–6691 (2020).
26. B. Gao, W. T. Gong, Q. L. Zhang, J. W. Ye, G. L. Ning, "A selective "turn-on" fluorescent sensor for Hg^{2+} based on "reactive" 7-hydroxycoumarin compound," *Sens. Actuators B* **162**, 391–395 (2012).
27. Y. Hou, Y. Chen, X. Y. Guo, W. Liu, C. C. Lv, Y. L. Xu, Y. Jin, B. X. Li, "Aggregation-induced chemiluminescence system for sensitive detection of mercury ions," *Anal. Bioanal. Chem.* **413**, 625–633 (2021).
28. L. Shi, F. J. Jia, L. Wang, M. Jalalah, M. S. Al-Assiri, T. Gao, F. A. Harraz, G. X. Li, "Fabrication of an artificial ionic gate inspired by mercury-resistant bacteria for simple and sensitive detection of mercury ion," *Sens. Actuators B* **326**, 128976 (2021).
29. M. Shellaiah, K. W. Sun, "Progress in metal-organic frameworks facilitated mercury detection and removal," *Chemosensors* **9**, 101 (2021).
30. A. Lopreside, L. Montal, B. J. Wang, A. Tassoni, M. Ferri, M. M. Calabretta, E. Michelini, "Orthogonal paper biosensor for mercury (II) combining bioluminescence and colorimetric smartphone detection," *Biosens. Bioelectron.* **194**, 113569 (2021).
31. K. Y. Zhang, Y. X. Sang, Y. D. Gao, Q. X. Sun, W. N. Li, "A fluorescence turn-on CDs-AgNPs composites for highly sensitive and selective detection of Hg^{2+}," *J. Hazard. Mater.* **264**, 120281 (2022).
32. M. Wang, W. Y. Feng, J. W. Shi, F. Zhang, B. Wang, M. T. Zhu, B. Li, Y. L. Zhao, Z. F. Chai, "Development of a mild mercaptoethanol extraction method for determination of mercury species in biological samples by HPLC–ICP-MS," *Talanta* **71**, 2034–2039 (2007).
33. M. Liu, C. S. Zhang, F. F. Liu, "Understanding wax screen-printing: A novel patterning process for microfluidic cloth-based analytical devices," *Anal. Chim. Acta* **891**, 234–246 (2015).
34. T. V. Ramakrisiina, G. Aravamudan, M. Vijayakumar, "Spectrophotometric determination of mercury(II) as the ternary complex with rhodamine 6G and iodide," *Anal. Chim. Acta* **84**, 369–375 (1976).
35. M. Barzan, F. Hajiesmaeilbaigi, "Investigation the concentration effect on the absorption and fluorescence properties of Rhodamine 6G dye," *Optik* **159**, 157–161 (2018).
36. G. H. Chen, W. Y. Chen, Y. C. Yen, C. W. Wang, H. T. Chang, C. F. Chen, "Detection of mercury (II) ions using colorimetric gold nanoparticles on paper-based analytical devices," *Anal. Chem.* **86**, 6843–6849 (2014).